Boosting Oxygen Evolution Reaction Induced by Carbon Sacrificial Strategy Based on FeNi2B@C/NF Core-shell Electrocatalyst

Yajuan Zhang [1, 2], Xingwei Shi [1, a, *], Xu Hui [2], Suojiang Zhang [1]

[1] Center of Ionic Liquids and Low Carbon Energy, Institute of Process Engineering, Chinses Academy of Sciences, Beijing, China;

[2] Key Laboratory of Low Carbon Energy and Chemical Engineering of Gansu Province, College of Petrochemical Technology, Lanzhou University of Technology, Lanzhou, China.

[a] xwshi@ipe.ac.cn

Abstract. Developing highly efficient and low-cost oxygen evolution reaction (OER) electrocatalysts under large current densities is attractive but challenging. To address this, we designed a novel Fe-doped carbon shell encapsulated nickel-boron core-shell heterostructure electrocatalyst (Fe-Ni_2B@C/NF) on nickel foam. The electronic structure of Ni_2B is effectively modulated by Carbon Sacrificial Strategy and the electron-donating characteristics of Fe, resulting in an upward shift of the d-band center. This modulation enhances the catalytic activity for OER by weakening the adsorption of oxygen-containing intermediates. In 1 M KOH solution, the Fe-Ni_2B@C/NF catalyst demonstrates remarkable performance with an overpotential of 208 mV at 10 mA cm^{-2} and excellent durability, outperforming commercial IrO_2. Additionally, when integrated into an anion exchange membrane (AEM) electrolyzer, the catalyst achieves a current density of 2000 mA cm^{-2} at a low voltage of 1.59 V, maintaining stability for over 1000 hours. Density functional theory (DFT) calculations further reveal that the core-shell heterostructure facilitates charge transfer between the carbon shell and Fe-Ni_2B core, reducing the energy barrier for OER intermediates and enhancing catalytic efficiency. This study provides a novel approach to developing efficient electrocatalysts with high catalytic activity and long-term durability at a large current density.

Keywords: AEM; Water electrolysis technology; Sacrificial carbon; Core-shell structure, OER.

1. Introduction

Electrically-driven water splitting for clean hydrogen energy is considered one of the most promising green and sustainable energy conversion technologies [1-3]. However, low-cost, high-efficiency hydrogen production is essential for the widespread development of water electrolysis. Anion exchange membrane (AEM) water electrolysis technology is a new generation of water electrolysis technology that combines the advantages of the low-cost non-precious metal catalysts and no titanium components of alkaline water (ALK) electrolysis technology and the high current density, high hydrogen purity, fast response, and high renewable energy suitability of proton exchange membrane (PEM) water electrolysis technology[4]. Its development is of great significance for realizing large-scale and cheap hydrogen production from renewable energy sources. However, as an alkaline electrolytic water system, AEM electrolysis technology still has the problem of slow catalytic reaction kinetics[5].

To solve this problem, herein, we developed a novel Fe-doped carbon shell encapsulated nickel-boron core-shell heterostructure electrocatalyst (Fe-Ni2B@C/NF) on nickel foam via a simple electroless plating and annealing process. Benefiting from the carbon sacrifice and the electron-donating properties of Fe, the electronic structure of Ni_2B is effectively regulated, resulting in an upward shift of the d-band center. This modulation weakens the adsorption of oxygen-containing intermediates and significantly enhances the electrocatalytic activity for OER. In a 1M KOH alkaline medium, the Fe-Ni2B@C/NF catalyst demonstrates remarkable performance with a lower OER overpotentials (η_{10}=208 mV), a small Tafel slope (49 mV dec–1) and excellent durability, surpassing the commercial IrO2. Moreover, the anion exchange membrane electrolyzer

utilizing Fe-Ni2B@C/NF as the anode catalyst and 20% Pt/C as the cathode catalyst exhibits exceptional electrolysis performance, achieving a current density of up to 2000 mA cm−2 at a low voltage of only 1.59 V, while maintaining high durability for over 1000 hours. DFT calculations reveal that core-shell heterostructures facilitates charge transfer from carbon shell and Fe atoms to pristine Ni2. This leads to an upshift in the d-band center of Fe-Ni2B@C/NF, thereby reducing the surface energy barrier, enhancing the adsorption of H2O and containing-oxygen intermediates.

2. Results and discussion

2.1 Synthesis, morphology and structure characterization

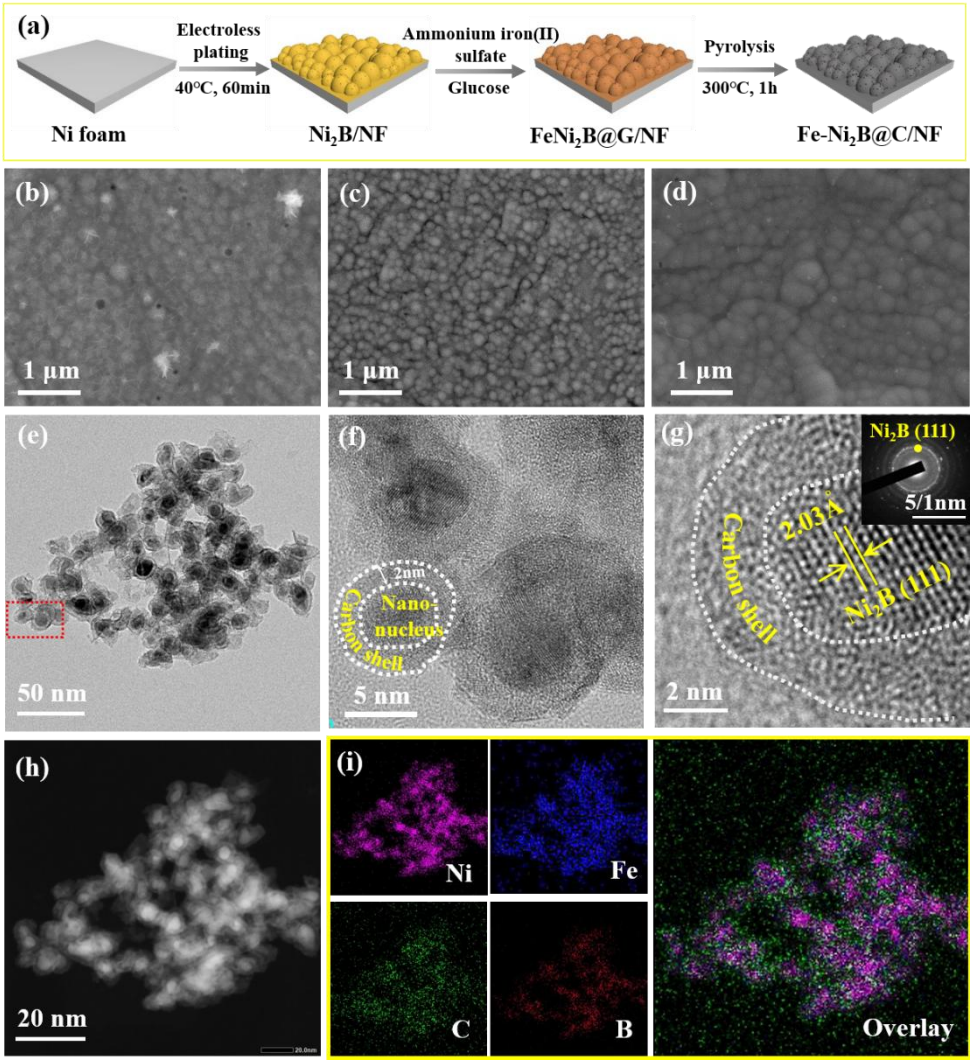

Figure 1. (a) Schematic diagram depicting the synthesis of Fe-Ni2B@C/NF electrodes. SEM images of (b) Fe-Ni2B@C/NF, (c) Fe-Ni2B/NF, and (d) Ni2B@C/NF electrodes. (e, f) TEM and (g) HR-TEM images of Fe-Ni2B@C/NF (insert SEAD pattern shows (111) and (121) planes). (h) HAADF-STEM image and the corresponding (i) STEM-EDX elemental mapping, and the overlay of the Ni, Fe, B, and C elements.

The synthesis of Fe-Ni2B@C/NF core-shell heterostructure catalysts involve two primary stages: nucleation and carbon shell encapsulate (Figure 1a). Specifically, the process begins with the formation of Ni-B/NF precursor on the surface of nickel foam (NF) using a simply electroless plating technique. The Ni-B/NF precursor is immersed in transparent solution containing glucose and ammonium ferrous sulfate, followed by annealing treatment. During the annealing process, Ni^{2+} and $Fe2^{+}$ are carbothermally reduced to metallic Ni, Fe leads to their rearrangement and the

formation of the Fe-Ni_2B crystalline structure and Fe doped carbon shell. Scanning electron microscope (SEM) images reveal that both the Fe-Ni_2B@C/NF and Ni_2B@C/NF shows uniformly dispersed irregular spherical nanoparticles with no visible cracks, agglomerations or defects across a wide coverage range (Figure1 b and d). These findings indicate that separating the nucleation and carbon shell encapsulation processes contributes to enhanced thermal stability of the materials. Conversely, Fe-Ni_2B/NF nanoparticles exhibit agglomeration and stacking (Figure 1c), confirming that carbon materials can improve dispersivity of metal borides, thus increasing the contact area between the catalyst and the electrolyte.

To investigate the internal microstructure of the Fe-Ni_2B@C/NF catalysts, transmission electron microscopy (TEM) was employed. As shown in Figure 1e, low magnification TEM image confirms that the nanoparticles are well-maintained with a size of ~10 nm. Enlarging the image of mark the square area, we can find Fe-Ni_2B nanonucleus widely distributed within the carbon skeleton, with the thickness of the translucent carbon shell being ~2 nm (Figure 1b). High-resolution TEM (HR-TEM) images distinctly exhibit an interface, with one side corresponding to the (111) plane of Ni2B, a lattice spacing of 2.03 Å, while the opposing side is assigned to the amorphous carbon shell (Figure 1g). Selected electron diffraction (SAED) pattern (inset Figure 1g) exhibits a set of diffraction ring corresponding to the (111) crystal plane of Ni2B, further confirming that Fe without destroying the crystal structure of Ni_2B. This result aligns with the XRD and TEM analyses. High-angle annular dark field scanning TEM (HAADF-STEM) (Figure h) and STEM-EDX element mapping (Figure i) confirm that the Fe-Ni_2B core is effectively encapsulated within the carbon skeleton. Additionally, the Ni and B elements are concentrated in the Fe-Ni_2B nanoparticles and C element is located in the carbon shell layer, whereas Fe is distribute throughout the sample, which suggests that Fe has a dual role both regulating the structure of Ni_2B and C shells. The above investigation demonstrate the Fe-Ni_2B@C/NF core-shell heterostructure electrocatalyst is successfully synthesized.

2.2 Water electrolysis performance of catalysts in AEM cell.

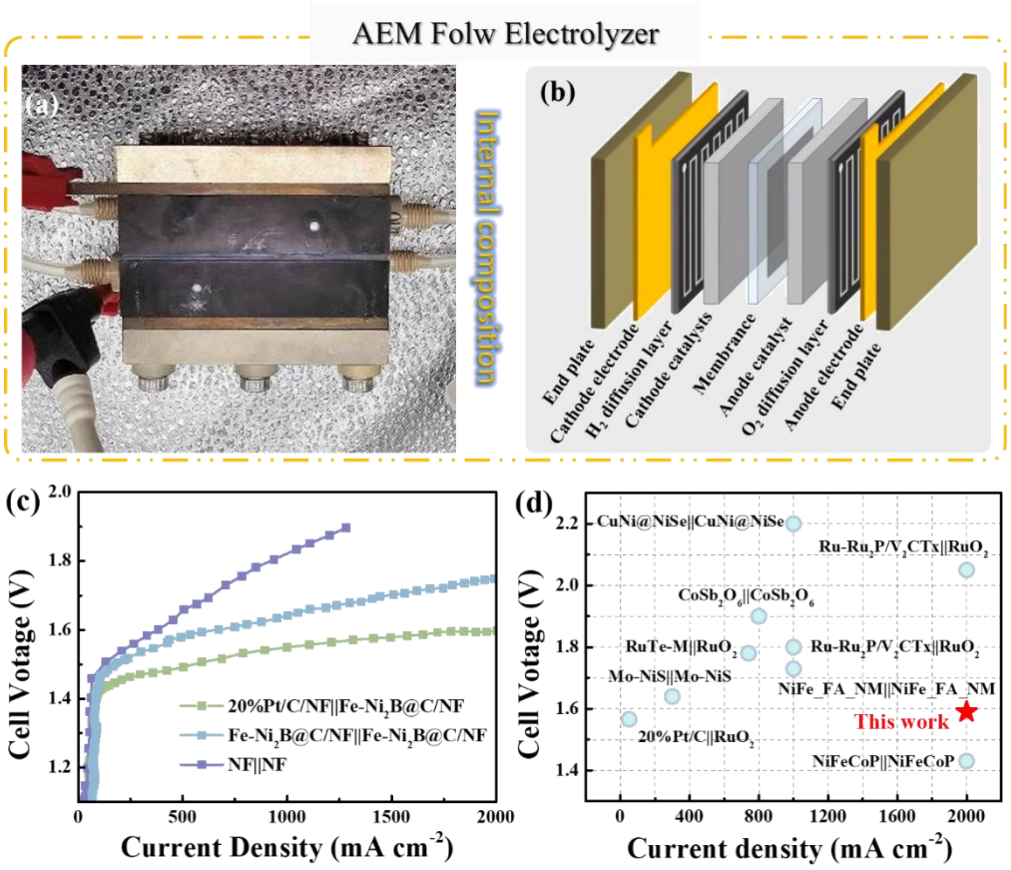

Figure 2. (a) Picture of AEM water electrolyzer and (b) schematic diagram of constitute AEM water electrolyzer. (c) Polarization curve of Fe-Ni2B@C/NF||Fe-Ni2B@C/NF, 20%Pt/C/NF||Fe-Ni2B@C/NF and NF||/NF electrode. (d) A comparsion for our design electrolyzer and the state of-the-art reported electrolyzers.

A high current density ($\geqslant$500 mA cm^{-2}) is often required for large-scale water electrolysis to produce hydrogen [6]. Thus, the feasibility studies were carried out for the $FeNi_2B$@C/NF catalysts in 1M KOH electrolyte. As illustrates in Figure 2a and b, the AEM water electrolysis device's internal structure is mainly made up of an anion exchange membrane, anode and cathode catalyst layers, and gas diffusion layer. Water electrolysis generates OH^- that may cross the membrane and transmit charge evenly to both sides of the cell. The polarization curves at room temperature indicate that the electrolytic cell with 20%Pt/C/NF‖$FeNi_2B$@C/NF exhibits significantly superior performance. It achieved high electrolytic current densities of 1/2 A cm^{-2} at only 1.54/1.59 V, respectively (Figure 2c). Simultaneously, our electrolyzer surpasses the energy efficiency of state-of-the-art electrolyzers reported for hydrogen production (Figure 2d), affirming the potential of FeNi2B@C/NF for energy-efficient water electrolysis.

2.3 The calculations of density functional theory (DFT)

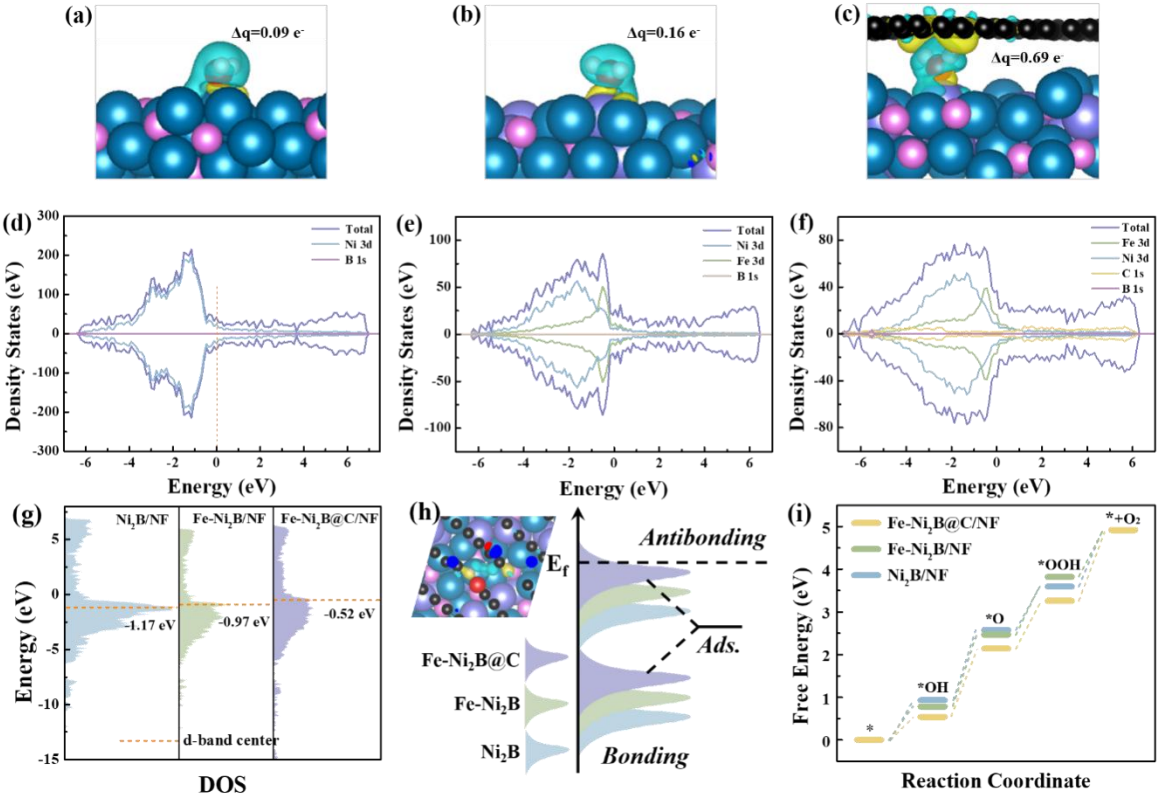

Figure 3. Theoretical calculations. Charge density differences of (a) Ni2B/NF, (b) Fe-Ni2B/NF and (c) Fe-Ni2B@C/NF, as well as their (d-f) density of states (DOS) the total DOS for the electrode, and (g) d-band center. (i) OER Gibbs free energy diagram for the FeNi2B@C/NF, FeNi2B/NF and Ni2B/NF.

Density functional theory (DFT) calculations were performed to further elucidate the effect of core-shell heterostructures construction on the improve OER performance. Figure 3a-c depicts the charge density differences for the Ni_2B/NF, Fe-Ni_2B/NF and Fe-Ni_2B@C/NF electrode, highlighting the effects of Fe doping and carbon shell on the electronic properties of catalysts. For the Fe-Ni_2B@C/NF electrode, charge transfer occurs between the Fe-Ni_2B/NF core and the carbon shell, amounting to a net transfer of 0.69 e-, with a notable charge accumulation on the carbon shell side. In comparison, the net charge transfers for the Fe-Ni_2B/NF and Ni_2B/NF electrodes are 0.16 e- and 0.09 e-, respectively, with charge transfer primarily occurring at the surface/interface of the

metallic boride. Additionally, the density of states (DOS) was calculated to further elucidate the enhanced electronic transfer for Fe-Ni_2B@C/NF. Figure 3d-f illustrate that the total DOS for the three materials aligns closely aligned around the Fermi energy level, confirming their inherent metallic nature [7]. Notably, the DOS of Fe-Ni_2B@C/NF consists of three primary components: Ni, Fe, and carbon. The d orbitals of Ni and Fe make the predominant contribution, while the p orbital of carbon displays a continuous state. In contrast, the DOS of Fe-Ni_2B/NF is dominated by contributions from Ni and Fe, whereas Ni_2B/NF primarily from Ni alone. This indicates that Fe-Ni_2B@C/NF facilitates greater electronic transfer to the carbon layer compared to the surface electron counts of the Fe-Ni_2B/NF and Ni_2B/NF. This electron transfer leads to the hole accumulation on Fe-Ni_2B, optimizing the binding energy for OER reaction intermediate and thereby demonstrating enhanced OER activity [8].

The d-band density of states for all electrocatalysts is illustrated in Figure 3g. In contrast to pristine Ni_2B/NF (-1.17 eV), an upshift in the d-band center is observed for both Fe-Ni_2B/NF (-1.17 eV) and Fe-Ni_2B@C/NF (-0.52 eV). Obviously, the d-band center of Ni_2B can be effectively adjusted through the formation of core-shell heterostructures using Fe doped and carbon shell. Upward shift of the d-band center tends to weaken the interaction between transition-metal d states and containing-oxygen intermediates (Figure 3h), leading to more moderate adsorption and desorption energies. This effect influences the Gibbs free energy (ΔG), which in turn affects the electrocatalytic performance. To further verify the intrinsic effects of the core-shell heterojunction on OER, the ΔG values for each containing-oxygen intermediates were calculated and are shown in Figure 3i. The transition from ΔG*O to ΔG*OOH presents the largest energy barrier, identifying this step as the potential OER-determining step (PDS) [9]. The adsorption free energy of ΔG*OOH is critical for determining the overpotential. The theoretical overpotentials of $FeNi_2B$@C/NF, $FeNi_2B$/NF, and Ni_2B/NF are 0.38 eV, 0.45 eV, and 0.68 eV, respectively. The results are consistent with the experiments data, indicating that $FeNi_2B$@C/NF displays the lowest overpotential, thus the best OER catalytic activity.

3. Summary

In summary, the Fe-Ni_2B@C/NF core-shell heterostructure electrocatalyst exhibits exceptional performance for OER, characterized by its low overpotential (η_{10}=208 mV), high current density (j_{max}=2000 mA cm^{-2}), and impressive durability (over 1000 hours). The strategic modulation of the electronic structure through Fe doping and carbon shell encapsulation effectively optimizes the d-band center, leading to improved electrocatalytic properties, which were confirmed by XPS, UPS and DFT. AEM electrolyzers using 20%Pt/C‖$FeNi_2B$@C/N electrode demonstrate industrial-scale high a current density of 2000 mA cm^{-2} and maintain this activity for over 1000 hours. These results underscore the potential of transition metal borides, particularly when integrated with carbonaceous materials, in advancing non-precious metal catalysts for alkaline water electrolysis. This work not only contributes to the fundamental understanding of catalyst design but also paves the way for the large-scale application of cost-effective and efficient electrocatalysts for sustainable hydrogen production.

References

[1] Z. Chen, R. Zheng, M. Graś, W. Wei, G. Lota, H. Chen, B.-J. Ni, Tuning electronic property and surface reconstruction of amorphous iron borides via W-P co-doping for highly efficient oxygen evolution, Applied Catalysis B: Environmental, 288 (2021).

[2] Y. Sun, Y. Zhao, X. Deng, D. Dai, H. Gao, An efficient amorphous ternary transition metal boride (WFeNiB) electrocatalyst for oxygen evolution from water, Sustainable Energy & Fuels, 6 (2022) 1345-1352.

[3] N. Xu, G. Cao, Z. Chen, Q. Kang, H. Dai, P. Wang, Cobalt nickel boride as an active electrocatalyst for water splitting, Journal of Materials Chemistry A, 5 (2017) 12379-12384.

[4] J. Lee, H. Jung, Y.S. Park, S. Woo, N. Kwon, Y. Xing, S.H. Oh, S.M. Choi, J.W. Han, B. Lim, Corrosion-engineered bimetallic oxide electrode as anode for high-efficiency anion exchange membrane water electrolyzer, Chemical Engineering Journal, 420 (2021).

[5] D. Xu, M.B. Stevens, M.R. Cosby, S.Z. Oener, A.M. Smith, L.J. Enman, K.E. Ayers, C.B. Capuano, J.N. Renner, N. Danilovic, Y. Li, H. Wang, Q. Zhang, S.W. Boettcher, Earth-Abundant Oxygen Electrocatalysts for Alkaline Anion-Exchange-Membrane Water Electrolysis: Effects of Catalyst Conductivity and Comparison with Performance in Three-Electrode Cells, ACS Catalysis, 9 (2018) 7-15.

[6] Nsanzimana, J. M. V.; Gong, L.; Dangol, R.; Reddu, V.; Jose, V.; Xia, B. Y.; Yan, Q.; Lee, J. M.; Wang, X. Tailoring of Metal Boride Morphology via Anion for Efficient Water Oxidation. Adv. Energy Mater. 9, (2019) 1901503.

[7] B. Fei, Z. Chen, J. Liu, H. Xu, X. Yan, H. Qing, M. Chen, R. Wu, Ultrathinning Nickel Sulfide with Modulated Electron Density for Efficient Water Splitting, Advanced Energy Materials, 10 (2020).

[8] H. Liu, C. Xi, J. Xin, G. Zhang, S. Zhang, Z. Zhang, Q. Huang, J. Li, H. Liu, J. Kang, Free-standing nanoporous NiMnFeMo alloy: An efficient non-precious metal electrocatalyst for water splitting, Chemical Engineering Journal, 404 (2021).

[9] X. Wang, P. Sun, H. Lu, K. Tang, Q. Li, C. Wang, Z. Mao, T. Ali, C. Yan, Aluminum-Tailored Energy Level and Morphology of Co(3-) (x) Al(x) O(4) Porous Nanosheets toward Highly Efficient Electrocatalysts for Water Oxidation, Small, 15 (2019) e1804886.